Green Chemistry

PAPER

View Article Online
View Journal | View Issue

Cite this: *Green Chem.*, 2025, **27**, 7564

High ionic conductivity conjugated artificial solid electrolyte interphase enabling stable lithium metal batteries†

Dong Yan,[a] Yuhao Ma,[a] Hao Wang,[a] Weishang Jia,[b] Xiaobin Niu,[a] Haibo Wang,*[c] Wei Zou*[d] and Liping Wang *[a]

Lithium metal batteries (LMBs) are promising for next-generation high-energy-density batteries but suffer from severe interface instability on reactive Li metal, resulting in poor cycling performance and resource inefficiency. In this study, we present a durable artificial solid electrolyte interphase (SEI) layer (composed of organic conjugated polyacrylonitrile (CPAN) and uniformly dispersed inorganic ZnO nanoparticles, denoted as CPAN@ZnO) using an eco-friendly approach, with reduced energy consumption and minimized thermal degradation byproducts. The unique conjugated structure of CPAN exhibits homogeneous surface electrostatic potential (ESP) distribution. When coupled with lithiophilic ZnO, this interaction induces more homogeneous Li deposition and inhibits dendrite growth. Additionally, its great binding energy with Li and rapid ion migration pathways effectively promote the de-solvation of Li^+ and enhance interfacial transport kinetics. Therefore, the CPAN@ZnO SEI exhibits high ionic conductivity, suppressing "dead Li" and dendrite, thus enhancing interface stability and extending the Li anode lifespan. As a result, the CPAN@ZnO@Li symmetrical cell achieves an ultralong cycling life of over 5400 h with a low overpotential, showcasing exceptional cycling stability. Furthermore, the Li-limited full cell NCM811||CPAN@ZnO@Cu (N/P = 0.6) delivers stable cycling over 100 cycles with a capacity retention of 88.8%. This work provides valuable insights into high ionic conductivity SEI design for stable cycling performance of Li-limited LMBs, reducing reliance on anode mining and mitigating environmental impacts from electrode material production, thereby contributing to resource sustainability.

Received 13th March 2025,
Accepted 22nd May 2025

DOI: 10.1039/d5gc01282a

rsc.li/greenchem

Green foundation

1. We propose an innovative SEI layer, which is fabricated through a sustainable strategy involving a mild annealing-cyclization process (260 °C for 1 h), reducing energy consumption and minimizing thermal degradation byproducts compared to conventional methods.
2. The CPAN@ZnO SEI, with high ionic conductivity and electronic insulation, enables uniform bottom-top Li deposition, and improves the interface stability of Li metal, thus enhancing the cycling stability of Li-limited batteries.
3. This work provides valuable insights into high ionic conductivity SEI design for stable cycling performance of Li-limited LMBs, reducing reliance on anode mining and mitigating environmental impacts from electrode material production, thereby contributing to resource sustainability.

1. Introduction

Lithium metal batteries (LMBs) are widely regarded as the "holy grail" of secondary batteries due to their high specific capacity (3860 mA h g^{-1}) and excellent high energy density (with a gravimetric energy density over 600 W h kg^{-1} in optimized cell designs).[1–5] However, the practical application of LMBs is hindered by significant interface instability issues on highly reactive Li metal anodes.[6–9] The interface instability includes uncontrollable dendrite growth, severe side reactions, and the formation of "dead Li", all of which contribute to poor cycling performance and resource inefficiency.[10–14] Specifically, the inhomogeneous nucleation and deposition of

[a]School of Materials and Energy, University of Electronic Science and Technology of China, Chengdu 610054, China. E-mail: lipingwang@uestc.edu.cn
[b]Key Laboratory of General Chemistry of the National Ethnic Affairs Commission, School of Chemistry and Environment, Southwest Minzu University, Chengdu, 610041, China
[c]College of Energy, Soochow University, Suzhou 215006, China. E-mail: wanghb@suda.edu.cn
[d]Lithium Resources and Lithium Materials Key Laboratory of Sichuan Province, Chengdu 610065, China. E-mail: zouwei@tianqi-welion.com

† Electronic supplementary information (ESI) available. See DOI: https://doi.org/10.1039/d5gc01282a

Li lead to severe Li dendrites, which can puncture the separator, causing short circuits and even fires.[15] Additionally, the accumulation of "dead Li" and continuous side reactions between Li metal and the electrolyte also degrade the performance of the battery.[16–19] Therefore, it is crucial to develop a stable and robust solid electrolyte interphase (SEI) with low electron conductivity and high ionic conductivity to enhance the interface stability of the Li metal anode, ultimately enabling high-performance LMBs.

In previous studies, tremendous efforts have been made to develop effective SEI layers for Li metal protection, such as the development of electrolyte additives, interfacial self-polymerization, metal passivation, *etc*.[20–26] Among the aforementioned strategies, organic polymers, such as polyethylene oxide (PEO), polyacrylonitrile (PAN), and polyvinylidene fluoride (PVDF), are widely preferred by researchers due to their superior mechanical properties, which make them effective in alleviating the volume expansion of Li metal.[27–31] Meanwhile, inorganic materials, including metal oxides and alloys, are frequently utilized for interface modification owing to their ability to regulate Li nucleation and growth.[32–36] Nevertheless, organic materials face limitations due to the non-uniform distribution of functional groups, resulting in uneven charge distribution and hindering homogeneous nucleation. Similarly, inorganic materials may also compromise interface stability due to issues such as volume expansion.[37] The optimal approach involves the effective integration of organic and inorganic materials, combining their respective advantages while mitigating their inherent limitations. Specifically, the flexibility of organic materials can be utilized to alleviate the volume expansion issues associated with inorganic materials, while the uniform dispersion and nucleation-inducing properties of inorganic materials help address the inhomogeneous Li deposition within the SEI formed by organic materials.

Hence, we propose a durable artificial SEI layer composed of conjugated organic polyacrylonitrile (CPAN) with uniformly dispersed inorganic ZnO nanoparticles, denoted as CPAN@ZnO. This innovative SEI layer was fabricated through a sustainable strategy involving a mild annealing-cyclization process (260 °C for 1 h), which reduces energy consumption and minimizes thermal degradation byproducts compared to conventional methods (Table S1†). The resulting CPAN@ZnO artificial SEI with dual functionality of promoting Li^+ transport and inducing uniform Li^+ deposition significantly enhances the stability of the Li metal surface and achieves stable long cycling performance of Li-limited LMBs.

2. Results and discussion

2.1 Design principle

As depicted in Fig. 1a, organic PAN was selected as the electrospinning polymer due to its low cost, finely modifiable spinnability and electron-rich nitrile group (–C≡N). $Zn(Ac)_2$ and *N*,*N*-dimethylformamide (DMF) were utilized as the metal ion additives and solvent, respectively. The CPAN@ZnO artificial SEI was initially synthesized by electrospinning, followed by mild thermal treatment in air to produce films with unique conjugated structures and a uniform distribution of ZnO particles. The as-prepared CPAN@ZnO layer exhibits high ionic conductivity due to the unique ion-conducting conjugated structure. In addition, it also exhibits a more homogeneous ESP distribution compared to the uncyclized PAN, which induces more homogeneous Li deposition and inhibits dendrite growth.[38]

The cyclization reaction of PAN was facilitated by the combined effects of heating and Zn^{2+}, leading to the cleavage of the triple bond in –C≡N and the formation of new –C=N– bonds (Fig. 1b). Apparently, the introduction of $Zn(Ac)_2$ resulted in darker fibre membranes under identical heating conditions, indicating a more profound cyclization of PAN under lower heating conditions (Fig. S1†). We found that the optimal $Zn(Ac)_2$ concentration was 600 mg per 10 mL of the precursor solution through Li||Cu cell testing (Fig. S2†). Simultaneous Thermal Analysis (STA) was performed to investigate the interaction between $Zn(Ac)_2$ and PAN. It revealed the catalytic effect of $Zn(Ac)_2$ on PAN cyclization (Fig. S3†). In the DSC curves (Fig. S3c†), the exothermic peak at 120 min (260 °C) corresponds to PAN cyclization, which shifts to earlier time and becomes sharper with $Zn(Ac)_2$ addition, indicating accelerated and enhanced cyclization. The corresponding mass loss profile (Fig. S3d†) reveals that PAN@$Zn(Ac)_2$ undergoes a notably greater mass loss (stage II), which corroborates the intensified dehydrogenation and cyclization of PAN. In addition, PAN@$Zn(Ac)_2$ undergoes an extra mass loss (stage III), corresponding to peak III in DSC curves, primarily attributed to the decomposition of $Zn(Ac)_2$.

As shown in Fig. 1c, the transformation in functional groups enables CPAN molecules to exhibit a more homogeneous ESP, resulting from the more homogenised charge distribution, which induces a more homogeneous Li deposition. Furthermore, this transformation not only enhances the mechanical properties and ESP, but also improves the Li^+ conductivity (Fig. S4†), which is much higher than that of traditional inorganic LiF and Li_2O.[39] Specifically, Li^+ selectively coordinates with the N atom in the –C=N– group and is further attracted to another electron-rich N atom, enabling Li^+ to freely jump between active sites on the conjugated CPAN scaffold, thus achieving higher Li^+ transport dynamics (Fig. S5†).[39,40] Moreover, it is electronically insulating, as evidenced by its current being below the detectable range of the test equipment. These properties selectively permit only Li^+ to transport through the artificial SEI layer to the Li metal surface, achieving uniform bottom to top deposition.

The binding energy calculations reveal that CPAN and ZnO exhibit strong binding energies with Li (−3.84 eV and −0.97 eV, respectively), which are substantially higher than those of uncyclized PAN-Li and common electrolyte solvents (DOL-Li and DME-Li) (Fig. 1d). The strong interactions promote the desolvation process of Li^+, thereby improving the dynamics and the rate capability of LMBs.[41] Based on the aforementioned characteristics, we designed and synthesized the organic–inorganic CPAN@ZnO artificial SEI featuring superionic conduc-

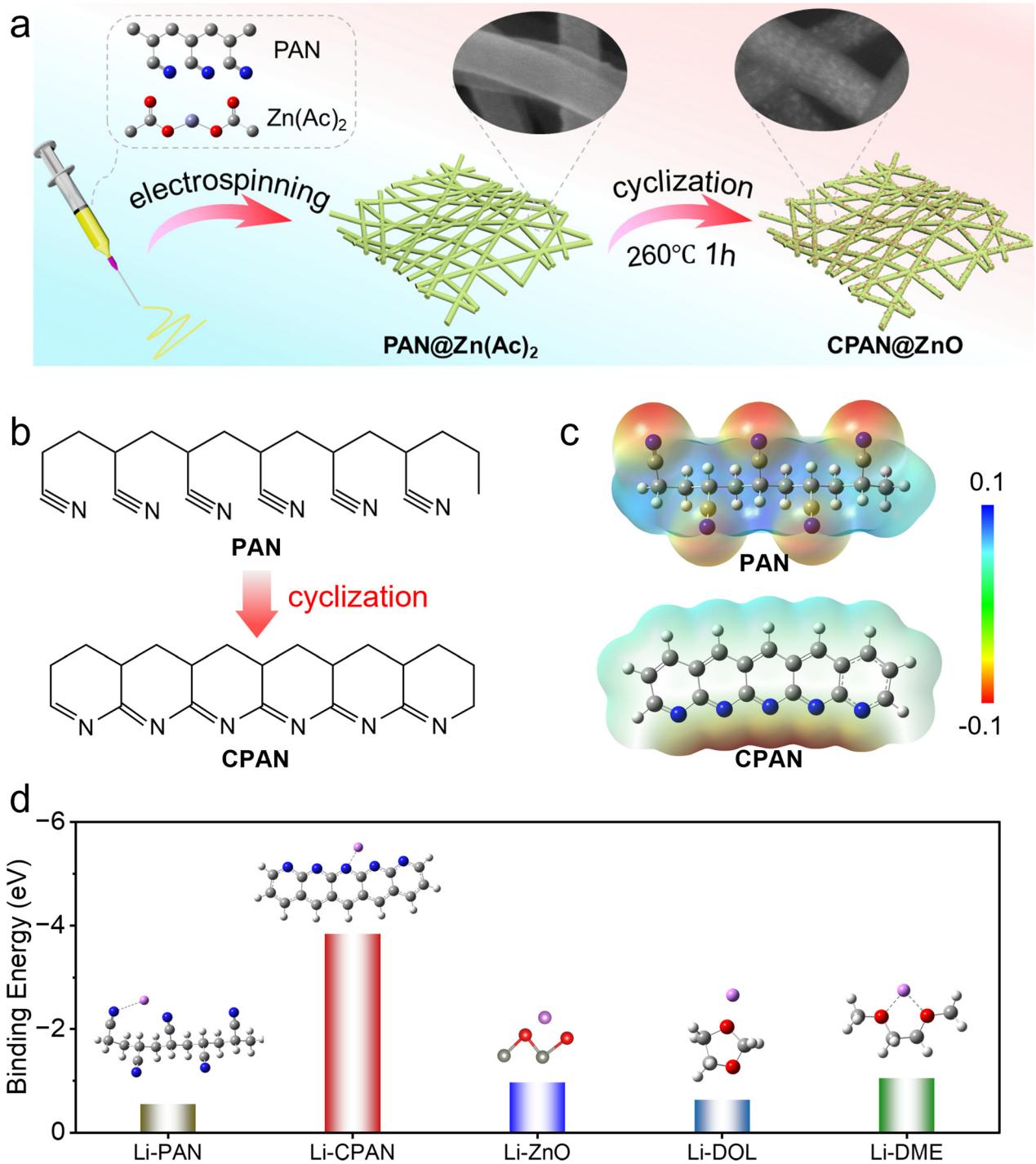

Fig. 1 Design principles. (a) Schematic illustration of the synthesis process of CPAN@ZnO. (b) Schematic diagram of the cyclization reaction of PAN. (c) ESP. (d) Binding energies of Li-PAN, Li-CPAN, Li-ZnO, Li-DOL, and Li-DME.

tivity, resulting in enhanced interface stability of the Li anode and improved cycling performance of LMBs.

2.2 Morphology and phase analysis

The micro-morphologies of the CPAN@ZnO and ZnO-free CPAN SEI are presented in Fig. 2a and Fig. S6,† respectively. Both artificial SEIs exhibit highly uniform nanofiber structures, with a diameter of approximately 200 nm and a thickness of about 10 μm (Fig. S7†). Notably, uniform ZnO nanoparticles are clearly visible on the CPAN@ZnO nanofibers. The well-defined nanoparticle–fibre composite structure is further confirmed by transmission electron microscopy (TEM). In the high-resolution TEM image (Fig. 2b), nanoparticles with a diameter of approximately 10 nm are observed with an interpla-

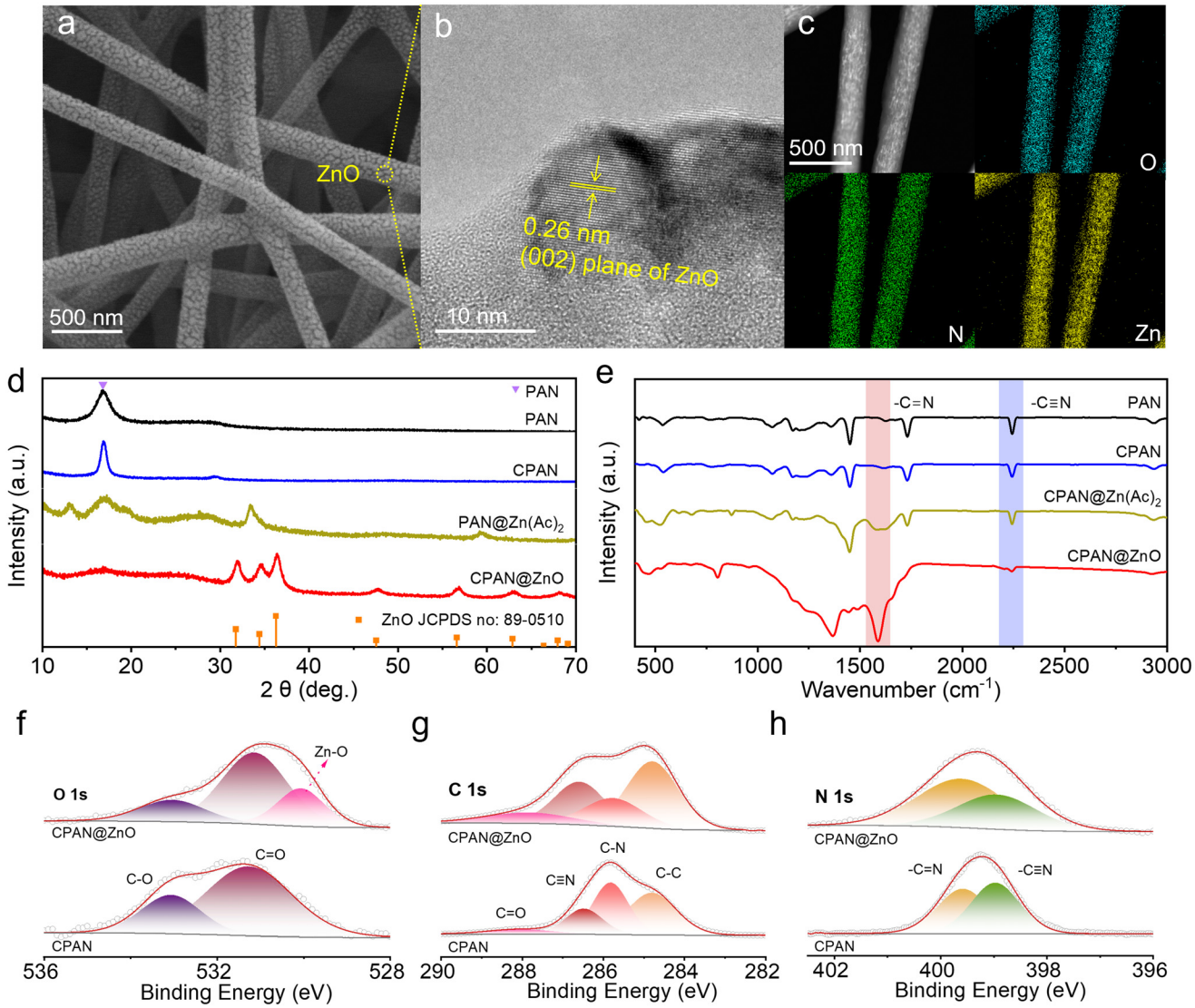

Fig. 2 Micromorphology and chemical composition analysis. (a) SEM image. (b) High-resolution TEM image. (c) Elemental mapping of CPAN@ZnO. (d) XRD patterns before and after the cyclization reaction. (e) FT-IR spectra before and after the cyclization reaction, and analysis of the degree of cyclization with/without zinc ions. (f–h) High-resolution XPS spectra for O 1s, C 1s and N 1s of CPAN@ZnO and CPAN before cycling.

nar distance of 0.26 nm, belonging to the (002) plane of ZnO. Additionally, elemental mappings of O, N, and Zn reveal an even distribution (Fig. 2c), indicating that ZnO nanoparticles are evenly dispersed on the nanofibers.

X-ray diffraction (XRD) reveals the phase differences between CPAN@ZnO and ZnO-free CPAN, as well as the phase evolution after annealing. As shown in Fig. 2d, the diffraction peaks of CPAN@ZnO are primarily assigned to hexagonal ZnO (JCPDS card number: 89-0510), while only the diffraction peaks of PAN are detected in the ZnO-free membranes before and after heating. It is noteworthy that the addition of $Zn(Ac)_2$ leads to a decrease in the intensity of the diffraction peak at 15°, corresponding to the (100) plane of PAN, which is caused by the deepening of the cyclization of the PAN molecule.[42,43] Meanwhile, the cyclization of PAN is further confirmed from the Fourier-transform infrared (FT-IR) spectra (Fig. 2e), where the peak of –C=N (approximately 1588 cm^{-1}) significantly intensifies after annealing and the peak of –C≡N (approximately 2244 cm^{-1}) notably decreases. Notably, the –C≡N peaks in CPAN@ZnO are largely converted into –C=N peaks, indicating that ZnO effectively catalyses PAN cyclization to form the conjugated structure with enhanced Li^+ migration and more uniform ESP distribution.

The surface chemical states of the artificial SEI were investigated by X-ray photoelectron spectroscopy (XPS), where both CPAN@ZnO and CPAN exhibit the presence of C, N, and O, and a distinct characteristic peak of Zn is detected in CPAN@ZnO (Fig. S8†). As revealed by the XPS spectra of O 1s (Fig. 2f), the O 1s spectra of CPAN@ZnO are deconvoluted into three peaks, with a symbolic peak for the ZnO phase near

530 eV.[44] Additionally, the XPS spectra of C 1s and N 1s further reveal significant differences of the surface chemical compositions between CPAN@ZnO and CPAN. In Fig. 2g, the characteristic peaks at 285.7 eV and 286.6 eV correspond to the C–N and C≡N groups, respectively.[40] Notably, CPAN@ZnO exhibits an enhanced C–N peak and a weakened C≡N peak compared to ZnO-free CPAN, which can be attributed to the ZnO-promoted cyclization reaction. Meanwhile, the degree of cyclization is semi-quantitatively analyzed using the high-resolution XPS spectra of N 1s and the corresponding fitting histograms (Fig. 2h and Fig. S9†), where the ratio of the cyclized C=N peak to the uncyclized C≡N peak in conjugated CPAN@ZnO is significantly higher than that in CPAN. These results collectively indicate that CPAN@ZnO has a higher degree of cyclization and a more extensive ion-conductive conjugated structure than ZnO-free CPAN.

2.3 Compatibility with Li metal

In order to evaluate the compatibility and the enhanced interface stability of CPAN@ZnO with Li metal, the Coulombic efficiency (CE) of Li||Cu cells and the cycling performance of symmetric cells were measured. As shown in Fig. 3a and Fig. S10,† the Li||CPAN@ZnO@Cu cell demonstrates significantly improved initial CE (ICE), average CE (ACE), and cycling stability compared to the bare Li||Cu cell, along with reduced cell polarization. These improvements suggest that the CPAN@ZnO layer effectively mitigates the formation of "dead Li" and suppresses interfacial side reactions. In addition, the Li@CPAN@ZnO symmetrical cell exhibits superior rate performance with higher electrochemical reversibility and faster Li^+ diffusion kinetics than the CPAN@ZnO-free counterpart. As depicted in Fig. 3b, the Li@CPAN@ZnO symmetrical cell shows the lowest overpotential at the same current density compared to Li@CPAN and bare Li symmetrical cells. Even at a high current density of 5 mA cm^{-2}, the Li@CPAN@ZnO symmetrical cell maintains a low polarization voltage of 60 mV. This performance is attributed to the unique conjugated structure and exceptional Li^+ conductivity of the CPAN@ZnO layer, which facilitates efficient Li^+ flux regulation and accelerates Li^+ diffusion. This work further evaluates the tolerability of CPAN@ZnO in harsh environments, demonstrating that Li@CPAN@ZnO shows a high critical current density of 8.2 mA cm^{-2}, significantly higher than those of Li@CPAN (4 mA cm^{-2}) and the bare Li electrode (3.6 mA cm^{-2}) (Fig. S11†), showing a great interface stability improvement of Li metal. We further investigated the battery kinetics, including deposition kinetics and ion transfer dynamics. The Li deposition kinetics were validated by deposition experiments on Li||Cu asymmetric batteries (Fig. S12†), where CPAN@ZnO@Cu has a lower Li nucleation overpotential (44 mV) and growth overpotential (16 mV) than bare Cu, implying an enhanced deposition and growth kinetics.[45] Additionally, the Tafel test in symmetric cells (Fig. S13†) shows that Li@CPAN@ZnO has a high exchange current density (1.3 mA cm^{-2}), which is 3 times that of Li@CPAN (0.4 mA cm^{-2}) and 6 times that of bare Li (0.2 mA cm^{-2}), highlighting the improved interfacial reactivity by the CPAN@ZnO artificial SEI.[46–48] Next, the ion transport dynamics were further corroborated by electrochemical impedance spectroscopy (EIS), which was shown in Fig. S14.† In detail, the corresponding equivalent circuit diagram and fitting results of EIS are presented in Fig. S15 and Table S2,† demonstrating that CPAN@ZnO effectively reduces the charge transfer resistance and improves the ion diffusion rate at the interface.[49–51] Additionally, the Li^+ transfer numbers (t_{Li^+}) were calculated. The Li@CPAN@ZnO symmetric cell exhibits a higher ion transportation dynamics (t_{Li^+} = 0.42), surpassing that of the bare Li battery (t_{Li^+} = 0.38). The EIS spectra of the initial and equilibrium states nearly overlap, as well as the current remaining almost unchanged after fast equilibrium, suggesting the excellent electrode stability of Li@CPAN@ZnO.[52] In conclusion, the CPAN@ZnO SEI significantly enhances both interface dynamics and stability, facilitating rapid Li^+ transport and lowering the energy barrier for uniform Li deposition.

The Li@CPAN@ZnO symmetrical cell achieves an ultralong cycling life of over 5400 h at a current density of 0.5 mA cm^{-2} and an areal capacity of 1 mA h cm^{-2}, with an ultra-low Li plating potential of 20 mV (Fig. 3c), which far exceeds the previous reports (Table S3†). The bare Li||Li battery (without CPAN@ZnO SEI protection) shows the poorest cycling performance, experiencing a short circuit at around 600 h. Additionally, the Li@CPAN@ZnO symmetric cell is able to cycle stably for approximately 3000 h with a low overpotential even under fast charging/discharging at a high current density of 1 mA cm^{-2} and a high loading of 4 mA h cm^{-2} (Fig. 3d). Conversely, the overpotential of the bare Li||Li cell gradually increases, accompanied by excessive dendrite growth, which ultimately leads to separator puncture and cell failure. The excellent long cycling stability confirms the positive effect of CPAN@ZnO on enhancing the interface stability of the Li metal anode, thus prolonging the stable cycle of LMBs.

The characterisation of the altered chemical state of the artificial SEI after Li deposition serves to validate the compatibility of CPAN@ZnO with Li metal. In the high-resolution XPS spectra of Zn 2p (Fig. 3e and Fig. S16†), both Zn $2p_{1/2}$ and Zn $2p_{3/2}$ peaks shift to lower binding energies after Li deposition, suggesting an increase in the electron density around the Zn atoms, which can be attributed to the formation of lithophilic LiZn alloys.[53,54] The chemical composition of the CPAN@ZnO artificial SEI is further confirmed from the Li 1s spectrum (Fig. 3f), along with the N 1s, O 1s, and F 1s spectra (Fig. S17†). In addition to the LiZn alloy, other inorganic compounds such as LiF, Li_3N, and Li_2O were detected, indicating that a dense SEI layer is formed by a combination of various inorganic compounds and organic conjugated CPAN, effectively isolating Li metal from the electrolyte and suppressing side reactions. It should be noted that the XRD pattern after Li deposition shows only diffraction peaks of ZnO in the CPAN@ZnO artificial SEI (Fig. S18†), with much weaker intensity than that before Li deposition, and no obvious crystalline diffraction peaks of other products. Combined with the XPS

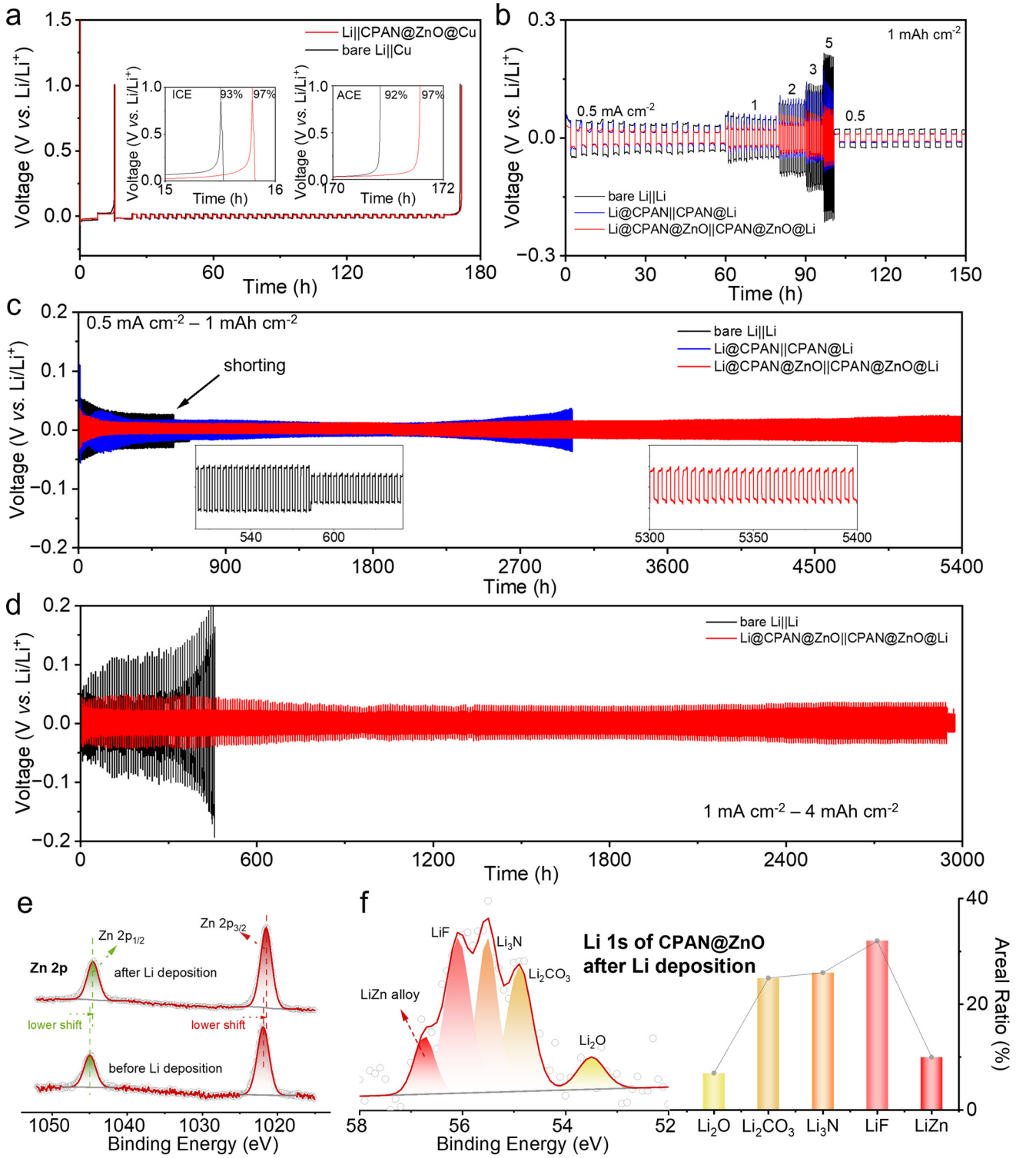

Fig. 3 Compatibility with Li metal. (a) Li||Cu test at 0.5 mA cm^{-2} with the modified Aurbach method. (b) Rate performance under 1 mA h cm^{-2} from 0.5 to 5 mA cm^{-2}. (c) Voltage profiles of Li symmetric cells at 0.5 mA cm^{-2} – 1 mA h cm^{-2}. (d) Voltage profiles of Li symmetric cells at 1 mA cm^{-2} – 4 mA h cm^{-2}. (e) High-resolution XPS spectra for Zn 2p of CPAN@ZnO. (f) High-resolution XPS spectra for Li 1s of CPAN@ZnO after Li deposition, along with the corresponding histograms of fitting peaks.

data, it is supposed that a partial ZnO–Li reaction yields minimal crystalline products, which verifies the stability of CPAN@ZnO. In addition, there is no obvious peak of Li metal, indicating that the residual metallic Li in the artificial SEI is negligible, demonstrating the efficient ion transport properties of the CPAN@ZnO SEI. Supplementarily, the weaker LiF peak

in the CPAN@ZnO layer compared to that in ZnO-free CPAN (Fig. S19†) suggests that the CPAN@ZnO layer effectively suppresses electrolyte contact with Li metal and subsequent detrimental decomposition.

The microscopic morphology of the cycled CPAN@ZnO artificial SEI was used to demonstrate its sustainability. As shown in Fig. S20a,† the fibrous structure of CPAN@ZnO remains well defined without noticeable "dead Li" accumulation and Li

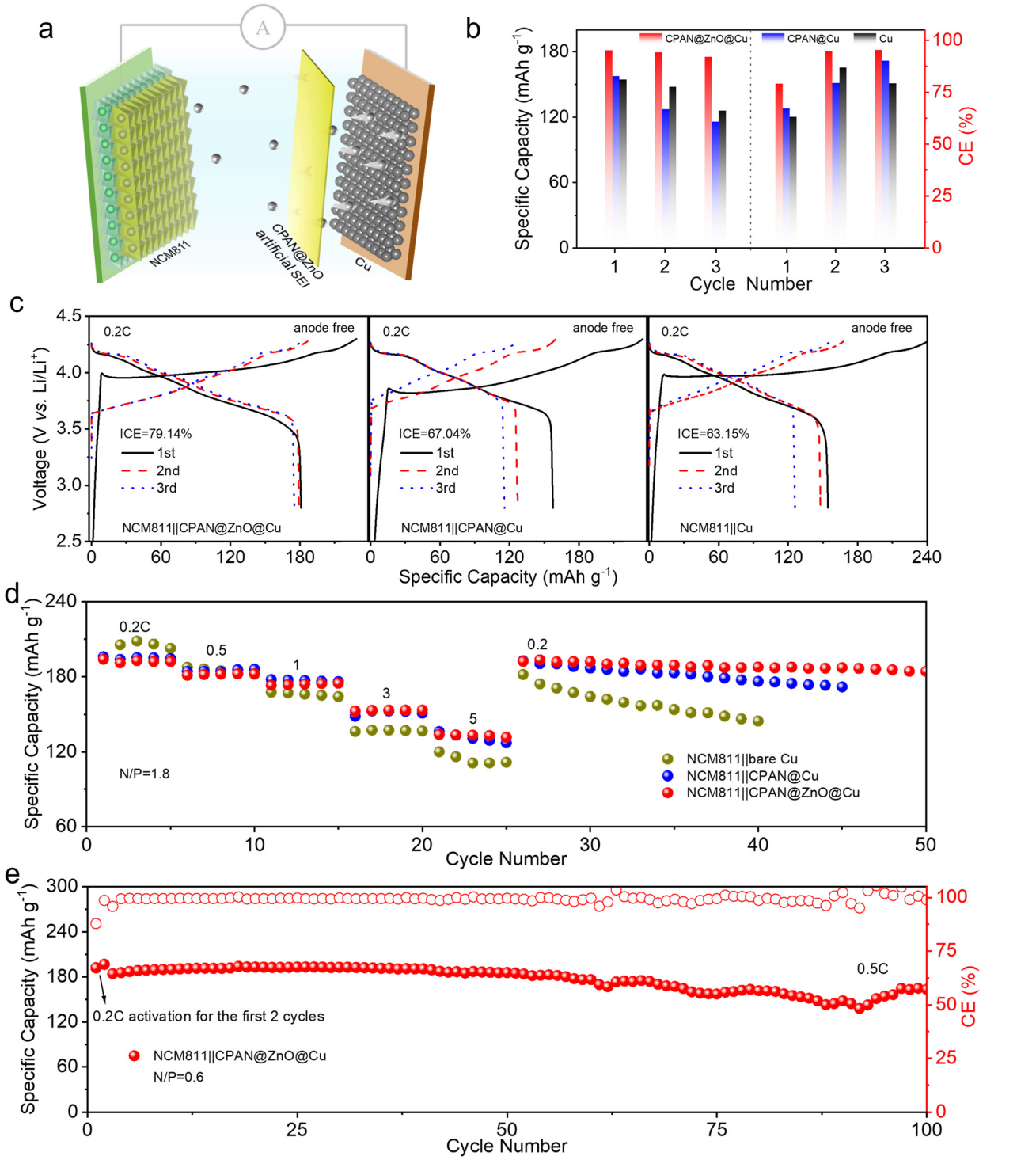

Fig. 4 Electrochemical performance of full cells composed of NCM811 and CPAN@ZnO@Cu/CPAN@Cu/bare Cu. (a) Schematic of anode-free full batteries. (b and c) Comparison of specific capacity and CE for the first 3 cycles of anode-free batteries, and the corresponding charging/discharging curves. (d) Rate performance (the CPAN@ZnO@Cu, CPAN@Cu, and bare Cu anode are pre-lithiated, N/P = 1.8). (e) Cycling performance at 0.5 C of NCM811||CPAN@ZnO@Cu with an ultra-low N/P ratio of 0.6.

dendrite. Moreover, obvious particles of Zn compounds were still observed on the nanofibers. The good morphological and structural retention of CPAN@ZnO indicates its electrochemical stability and long-term cycling sustainability. Furthermore, the surface morphology of Li metal after cycling further demonstrates the positive effect of the CPAN@ZnO SEI in enhancing the interface stability of Li metal. As depicted in Fig. S20b and S20c,† the high ionic conductivity of the CPAN@ZnO layer ensures that the cycled Li metal surface remains smooth and flat, closely resembling the original Li metal, which avoids the surface unevenness and cracking caused by the excessive inactivation of "dead Li".[30]

2.4 Electrochemical performance of Li-limited LMBs

The high ionic conductivity of CPAN@ZnO SEI was further explored for application in anode-free full cells. As shown in Fig. 4a, the anode-free full cells were assembled with the NCM811 cathode and the CPAN@ZnO@Cu, CPAN@Cu, or bare Cu anode. Initially, the specific capacity and CE of full cells with the three different Li-free anodes were compared and analysed. As shown in Fig. 4b and c, the anode-free NCM811||CPAN@ZnO@Cu full cell exhibits the highest ICE (79%), much higher than that of NCM811||CPAN@Cu (67%) and NCM811||bare Cu (63%), confirming the inhibition of "dead Li" and Li dendrites by CPAN@ZnO artificial SEI.

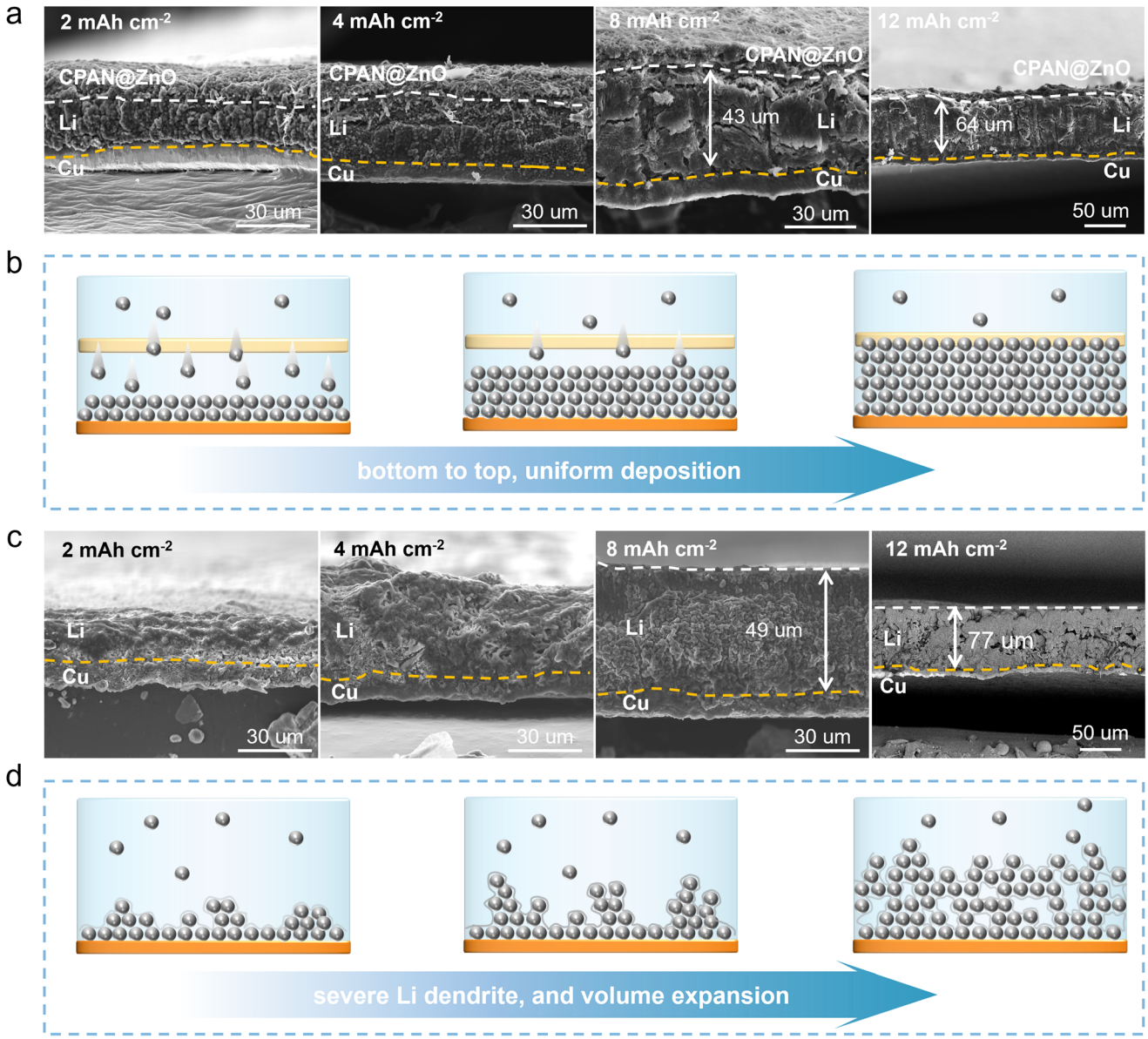

Fig. 5 Li plating behaviours. (a and b) Li deposition behaviour on CPAN@ZnO@Cu. The SEM cross-section at different deposition capacities from 2 to 12 mA h cm^{-2} and schematic diagrams of the corresponding deposition models. (c and d) Li deposition behaviour on bare Cu. The SEM cross section at different deposition capacities from 2 to 12 mA h cm^{-2} and schematic diagrams of the corresponding deposition models.

Meanwhile, CPAN@ZnO also enhances the discharge specific capacity and capacity retention of the anode-free full battery, further verifying its superior ionic conductivity and low Li residuals. To further optimize the cycling stability of the anode-free full cells, pre-lithiation of the Li-free anode was performed prior to cell assembly. The resulting rate performance is presented in Fig. 4d and Fig. S21.† The NCM811||CPAN@ZnO@Cu cell exhibits excellent reversible specific capacity, delivering a capacity of 133 mA h g^{-1} at a high rate of 5 C. Moreover, it maintains excellent electrochemical reversibility and stability, sustaining high-capacity stable cycling performance even after returning to 0.2 C from 5 C. However, NCM811||bare Cu exhibits poor electrochemical performance, with a 5 C capacity of only 111 mA h g^{-1}, and a rapid capacity decay for further cycling at 0.2 C. The long cycling performance at 0.5 C is depicted in Fig. S22;† the NCM811||CPAN@ZnO@Cu cell demonstrates excellent cycling durability, maintaining stable performance over 200 cycles with a capacity retention of 78.4%. More importantly, as presented in Fig. 4e, Fig. S23, and Table S4,† the NCM811||CPAN@ZnO@Cu cell with an ultra-low N/P ratio of 0.6 exhibits stable cycling performance at 0.5 C, maintaining a capacity retention of 88.8% over 100 cycles. These findings suggest that CPAN@ZnO holds significant application potential for high-energy-density Li-limited batteries.

2.5 Li plating behaviours

The modulation capacities of Li^+ using the CPAN@ZnO artificial SEI, including deposition and growth behaviours, were resolved through the cross-sectional morphology under different Li deposition capacities. In Fig. 5a and Fig. S24,† three well-defined layers of dissimilar substances are clearly visible following Li deposition: (1) the bottom layer corresponds to the Cu substrate, (2) the intermediate layer consists of densely packed deposited Li metal, (3) the fibrous top layer represents the electronically insulating CPAN@ZnO artificial SEI. It needs to be highlighted that the intermediate layer of deposited Li metal is densely arranged and free of dendrites. Additionally, the actual deposition thickness was further compared with the unmodified group to analyse the inhibitory effect of CPAN@ZnO on the volume expansion of Li. Even at a high deposition capacity of 12 mA h cm^{-2}, the actual deposition height of Li under the regulation of CPAN@ZnO@Cu is about 64 μm (Fig. 5a and Fig. S24†), which is markedly less than the value for the blank group (77 μm, Fig. 5c), effectively illustrating the modulation of Li deposition and suppression of volume expansion by CPAN@ZnO. From the EDS, it can also be concluded that Li is initially deposited on the Cu substrate rather than the CPAN@ZnO layer, and then gradually deposits upwards, achieving bottom-top, dendrite-free uniform deposition. In contrast, the Li deposition on bare Cu substrates exhibits pronounced holes, resulting in severe volume expansion (Fig. 5c). This gives a reasonable explanation for the poor cycling life of bare Li||Li and NCM811||Cu cells.

Overall, due to our superior design and successful fabrication of the CPAN@ZnO artificial SEI with electronic insulation and high ionic conductivity, we have achieved a uniform Li deposition from bottom to top, suppressing dendrite growth and side reactions, and ultimately improving the interface stability of the Li anode and realizing the stable cycling performance of LMBs.

3. Conclusions

In summary, we successfully synthesized durable CPAN@ZnO nanofibers by a green synthesis method with energy conservation and emission reduction. The as-prepared CPAN@ZnO, serving as an artificial SEI, possesses electronic insulation and fast ion migration properties, effectively alleviating the interface instability of the Li metal anode. In detail, the unique ion-conduction conjugated structure accelerates the interfacial Li^+ migration kinetics, suppresses the formation of "dead Li" and dendrites, and enables uniform bottom-top deposition. Thus, it enhances the interface stability of reactive Li metal and the cycling life of LMBs. As a result, the CPAN@ZnO@Li symmetrical cell achieves an exceptional cycling property of over 5400 h. The Li-limited NCM811||CPAN@ZnO@Cu full cell (N/P = 0.6) demonstrates stable cycling performance over 100 cycles with a capacity retention of 88.8% at 0.5 C, highlighting the application potential of CPAN@ZnO for high energy density batteries. Our work presents a simple and eco-friendly strategy to prepare a functional artificial SEI, which not only achieves high interfacial stability of Li metal but also enables stable cycling of Li-limited batteries, thus reducing the reliance on anode mining and promoting resource sustainability.

Author contributions

Dong Yan: writing – review & editing, writing – original draft, visualization, validation, investigation, and data curation. Yuhao Ma: methodology, investigation, and writing – original draft. Hao Wang: methodology, investigation, and writing – original draft. Weishang Jia: methodology, investigation, and writing – original draft. Xiaobin Niu: methodology, investigation, and writing – original draft. Haibo Wang: methodology, investigation, and writing – original draft. Wei Zou: methodology, investigation, and writing – original draft. Liping Wang: conceptualization, writing – review & editing, supervision, and funding acquisition.

Data availability

The data supporting this article have been included as part of the ESI.†

Conflicts of interest

There are no conflicts to declare.

Acknowledgements

This work was supported by the Beijing National Laboratory for Condensed Matter Physics (No. 2023BNLCMPKF015), the National Natural Science Foundation of China (No. 22322903), the Natural Science Foundation of Sichuan, China (No. 2023NSFSC1914), and the Jiangsu Province Carbon Peak and Neutrality Innovation Program (industry tackling on prospect and key technology) (No. BE2022002-3).

References

1 M. He, L. G. Hector, F. Dai, F. Xu, S. Kolluri, N. Hardin and M. Cai, *Nat. Energy*, 2024, **9**, 1199–1205.
2 Z. Li, G. Zhou, S. Li, H. Liu, L. Wang and H. Li, *Joule*, 2023, **7**, 2609–2621.
3 S. Li, H. Liu, L. Zheng, C. Ma, H. Yu, X. Wu, X. Niu and L. Wang, *Nano Energy*, 2024, **131**, 110234.
4 L. Wang, Z. Wu, J. Zou, P. Gao, X. Niu, H. Li and L. Chen, *Joule*, 2019, **3**, 2086–2102.
5 D. Di Lecce, V. Marangon, H.-G. Jung, Y. Tominaga, S. Greenbaum and J. Hassoun, *Green Chem.*, 2022, **24**, 1021–1048.
6 G. Liu, W. Wan, Q. Nie, C. Zhang, X. Chen, W. Lin, X. Wei, Y. Huang, J. Li and C. Wang, *Energy Environ. Sci.*, 2024, **17**, 1163–1174.
7 Y. Gu, E. You, J. Lin, J. Wang, S. Luo, R. Zhou, C. Zhang, J. Yao, H. Li, G. Li, W. Wang, Y. Qiao, J. Yan, D. Wu, G. Liu, L. Zhang, J. Li, R. Xu, Z. Tian, Y. Cui and B. Mao, *Nat. Commun.*, 2023, **14**, 3536.
8 Z. Huang, J. Lai, S. Liao, Z. Yu, Y. Chen, W. Yu, H. Gong, X. Gao, Y. Yang, J. Qin, Y. Cui and Z. Bao, *Nat. Energy*, 2023, **8**, 577–585.
9 Y. Zhan, Z. Liu, Y. Geng, P. Shi, N. Yao, C. Jin, B. Li, G. Ye, X. Zhang and J. Huang, *Energy Storage Mater.*, 2023, **60**, 102799.
10 L. Ma, J. Cui, S. Yao, X. Liu, Y. Luo, X. Shen and J. Kim, *Energy Storage Mater.*, 2020, **27**, 522–554.
11 W. Xu, J. Wang, F. Ding, X. Chen, E. Nasybulin, Y. Zhang and J. Zhang, *Energy Environ. Sci.*, 2014, **7**, 513–537.
12 H. Liu, Z. Wu, H. Wang, X. Niu, H. Li and L. Wang, *ACS Energy Lett.*, 2024, **9**, 4666–4672.
13 X. Han, X. Wang, M. Han and J. Sun, *Green Chem.*, 2020, **22**, 4252–4258.
14 S. Cho, D. Y. Kim, J. I. Lee, J. Kang, H. Lee, G. Kim, D. H. Seo and S. Park, *Adv. Funct. Mater.*, 2022, **32**, 2208629.
15 Y. Sun, J. Li, S. Xu, H. Zhou and S. Guo, *Adv. Mater.*, 2023, **36**, 202311687.
16 P. Molaiyan, S. Bhattacharyya, G. S. dos Reis, R. Sliz, A. Paolella and U. Lassi, *Green Chem.*, 2024, **26**, 7508–7531.
17 J. Sun, H. Zhou and Z. Huang, *Green Chem.*, 2024, **26**, 6926–6943.
18 L. Cao, M. Chu, Y. Li, X. Xu, Y. Qiu, Y. Dai, C. Sun, Z. X. Huang, X. L. Wu and H. Geng, *Adv. Mater.*, 2024, **36**, 2406034.
19 H. Liang, H. Liu, J. Guo, X. Zhao, Z. Gu, J. Yang, X. Zhang, Z. Liu, W. Li and X. Wu, *Energy Storage Mater.*, 2024, **66**, 103230.
20 C. Ma, S. Zou, Y. Wu, K. Yue, X. Cai, Y. Wang, J. Nai, T. Guo, X. Tao and Y. Liu, *Angew. Chem., Int. Ed.*, 2024, **63**, e202402910.
21 L. Yue, X. Wang, L. Chen, D. Shen, Z. Shao, H. Wu, S. Xiao, W. Liang, Y. Yu and Y. Li, *Energy Environ. Sci.*, 2024, **17**, 1117–1131.
22 X. Lu, Y. Wang, X. Xu, B. Yan, T. Wu and L. Lu, *Adv. Energy Mater.*, 2023, **13**, 2301746.
23 H. Wan, Z. Wang, W. Zhang, X. He and C. Wang, *Nature*, 2023, **623**, 739–744.
24 Y. Feng, Y. Li, J. Lin, H. Wu, L. Zhu, X. Zhang, L. Zhang, C. Sun, M. Wu and Y. Wang, *Nat. Commun.*, 2023, **14**, 3639.
25 S. Zhang, F. Sun, X. Du, X. Zhang, L. Huang, J. Ma, S. Dong, A. Hilger, I. Manke, L. Li, B. Xie, J. Li, Z. Hu, A. C. Komarek, H.-J. Lin, C. Kuo, C. Chen, P. Han, G. Xu, Z. Cui and G. Cui, *Energy Environ. Sci.*, 2023, **16**, 2591–2602.
26 H. Liang, H. Liu, X. Zhao, H. Lü, Z. Gu, J. Yang, Y. Chang, H. Yu, J. Zhang, J. Guo and X. Wu, *Energy Storage Mater.*, 2024, **71**, 103633.
27 Z. Liu, G. Li, M. Xi, Y. Huang, H. Li, H. Jin, J. Ding, S. Zhang, C. Zhang and Z. Guo, *Angew. Chem., Int. Ed.*, 2024, **63**, e202319091.
28 Y. Liu, W. Guan, S. Li, J. Bi, X. Hu, Z. Du, H. Du, W. Ai and W. Huang, *Adv. Energy Mater.*, 2023, **13**, 202302695.
29 J. Wan, X. Liu, T. Diemant, M. Wan, S. Passerini and E. Paillard, *Energy Storage Mater.*, 2023, **63**, 103029.
30 X. Zhang, C. Fu, S. Cheng, C. Zhang, L. Zhang, M. Jiang, J. Wang, Y. Ma, P. Zuo, C. Du, Y. Gao, G. Yin and H. Huo, *Energy Storage Mater.*, 2023, **56**, 121–131.
31 J. Sun, Y. Wang, Y. Li and W. Feng, *Sci. China Mater.*, 2024, **67**, 1393–1402.
32 J. Zhang, H. Chen, M. Wen, K. Shen, Q. Chen, G. Hou and Y. Tang, *Adv. Funct. Mater.*, 2021, **32**, 202110110.
33 H. Zhang, X. Liao, Y. Guan, Y. Xiang, M. Li, W. Zhang, X. Zhu, H. Ming, L. Lu, J. Qiu, Y. Huang, G. Cao, Y. Yang, L. Mai, Y. Zhao and H. Zhang, *Nat. Commun.*, 2018, **9**, 3729.
34 J. Liu, N. Pei, X. Yang, R. Li, H. Hua, P. Zhang and J. Zhao, *Energy Mater.*, 2023, **3**, 300024.
35 Y. Tan, Z. Liu, J. Zheng, Z. Ju, X. He, W. Hao, Y. Wu, W. Xu, H. Zhang, G. Li, L. Zhou, F. Zhou, X. Tao, H. Yao and Z. Liang, *Adv. Mater.*, 2024, **36**, 2404815.
36 Y. Zhao, D. Wang, Y. Gao, T. Chen, Q. Huang and D. Wang, *Nano Energy*, 2019, **64**, 103893.
37 X. Meng, S. Zhou, J. Li, Y. Chen, S. Lin, C. Han and A. Pan, *Adv. Funct. Mater.*, 2023, **34**, 2309350.
38 S. Ma, J. Zhao, Q. Gao, C. Song, H. Xiao, F. Li and G. Li, *Angew. Chem., Int. Ed.*, 2023, **62**, e202315564.

39 K. Wang, T. Zhao, R. Lv, W. Tang, T. Yu, G. Chen, L. Li, F. Wu and R. Chen, *Adv. Energy Mater.*, 2024, **14**, 2401281.
40 H. Liu, Y. Liao, C. Leung, Y. Zhang, Y. Yang, F. Liu, Y. Wei, C. Fan, S. Zhang, D. Wang, J. Yan, Q. Liu, C. Chung, Y. Ren, Y. Huang and J. Yang, *Adv. Energy Mater.*, 2024, **15**, 2402795.
41 H. Zhang, R. Guo, S. Li, C. Liu, H. Li, G. Zou, J. Hu, H. Hou and X. Ji, *Nano Energy*, 2022, **92**, 106752.
42 J. Zeng, G. Zhao, J. Liu, Y. Xiang and S. Guo, *Diamond Relat. Mater.*, 2024, **141**, 110588.
43 H. Zhu, Q. Chen, H. Malik, Y. Wang, J. He, B. Ma, X. Wang, H. Zhang, Y. Liu and J. Yu, *Polym. Degrad. Stab.*, 2024, **230**, 111082.
44 X. Chen, Y. Chen, L. Zhang, Z. Liu, E. Qiu, Q. Liu, M. D. Regulacio, C. Lin and D. Yang, *J. Colloid Interface Sci.*, 2023, **648**, 535–550.
45 K. Yan, Z. Lu, H. Lee, F. Xiong, P. Hsu, Y. Li, J. Zhao, S. Chu and Y. Cui, *Nat. Energy*, 2016, **1**, 16010.
46 M. Yang, Y. Wu, K. Yang, Z. Wang, T. Ma, D. Wu, F. Xu, L. Yang, P. Lu, J. Peng, Q. Gao, X. Zhu, Z. Jiang, L. Chen, H. Li and F. Wu, *Adv. Energy Mater.*, 2024, **14**, 202303229.
47 Z. Wen, W. Fang, F. Wang, H. Kang, S. Zhao, S. Guo and G. Chen, *Angew. Chem., Int. Ed.*, 2024, **63**, e202314876.
48 Z. Sun, Y. Wang, S. Shen, X. Li, X. Hu, M. Hu, Y. Su, S. Ding and C. Xiao, *Angew. Chem., Int. Ed.*, 2023, **62**, e202309622.
49 Z. Hao, C. Wang, Y. Wu, Q. Zhang, H. Xu, Y. Jin, J. Liu, H. Wang and X. He, *Adv. Energy Mater.*, 2023, **13**, 2204007.
50 H. Yao, F. Niu, C. Ma, X. You, D. Ning, J. Qian, M. Wang, Q. Duan, C. Yang, Q. Wu, J. Wang, J. Zhang, Z. Lu, C. Yang and W. Wu, *Adv. Funct. Mater.*, 2023, **34**, 2310711.
51 D. Yan, S. Xiao, X. Li, J. Jiang, Q. He, H. Li, J. Qin, R. Wu, X. Niu and J. S. Chen, *Energy Mater. Adv.*, 2023, **4**, 0012.
52 H. X. Yang, Z. K. Liu, Y. Wang, N. W. Li and L. Yu, *Adv. Funct. Mater.*, 2022, **33**, 2209837.
53 B. Cao, H. Liu, X. Zhang, P. Zhang, Q. Zhu, H. Du, L. Wang, R. Zhang and B. Xu, *Nano-Micro Lett.*, 2021, **13**, 202.
54 X. Fu, Y. Hu, W. Li, J. He, Y. Deng, R. Zhang and G. Chen, *Small*, 2024, **20**, 202405227.

